Exploring Process-Properties Relationships of 3D-Printed PLA: Towards Process-Informed Simulation and Design

Aaron Grant[1], Brett Ellis[2,3], Masoud Rais-Rohani[1,3], and Reza Hajiha[4]

[1]Mechanical Engineering, University of Maine, Orono, ME 04469
[2]Mechanical Engineering Technology, University of Maine, Orono, ME 04469
[3]Center for Additive Manufacturing of Metals (CAMM), University of Maine, Orono, ME 04469
[4]Alphastar Corp., Long Beach, CA 90804

ABSTRACT

The simulation of additively manufactured (AM) Polylactic Acid (PLA) tensile specimen is discussed. The procedure of evolution and use of a material definition for finite element simulation (FEA) of Polylactic Acid (PLA) printing is discussed, using the programs MCQ-Chopped, MCQ-Composites, ABAQUS, and GENOA.

Keywords: additive, simulation, polymer, abaqus, printing

1 INTRODUCTION

Capturing the relations between a manufacturing process and the properties imposed by the technique are key to being able to exploit the limits of that process. Process-Structure-Property-Performance (PSPP) relations, as shown in Figure 1, divide the aim of manufacturing into smaller goals which themselves need realization to achieve the overall aim.

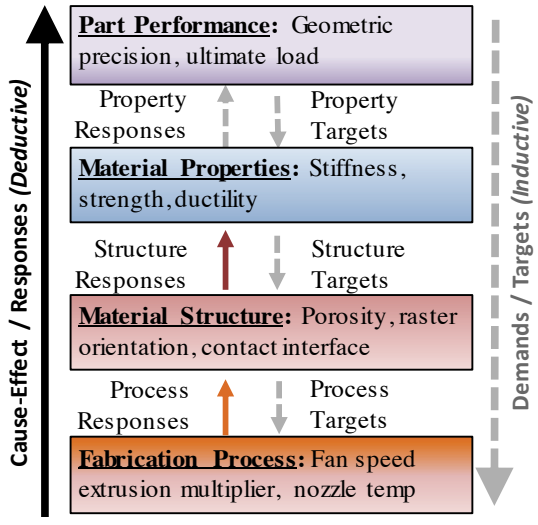

Figure 1: PSPP relations in a manufacturing environment

The reductions in lead times and geometric freedom offered by AM are unparalleled by any other manufacturing technique, however, the complexity of process-based degrade in AM hinders the practicality of even the most basic parts.

2 PROCESS-PROPERTIES MODELING

The software GENOA is a micromechanics modeling tool that can capture process-property degradation in an AM process, as outlined in Figure 2.

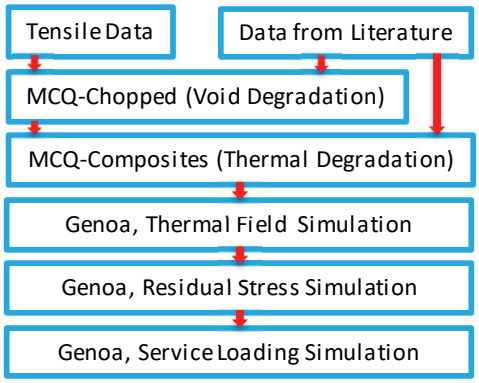

Figure 2: The procedure of process modeling using GENOA, MCQ-Chopped and MCQ-Composites

GENOA's capability has been used in qualification of AM processes for several AM materials, such as ULTEM 1010 [1], and ABS-CF13 [2]. This report aims to qualify a more mainstream AM material, PLA.

MCQ-Chopped uses a predictive algorithm to match tensile data by introducing of a damage model imposed on neat material properties, thereby including the effect of voids introduced by AM. Input data was augmented with data extracted from literature, extending the predictive model to predict response to an arbitrary loading. Moreover, MCQ-Composites extends the MCQ-Chopped model to include temperature dependency by coupling the model with a temperature-dependent Young's modulus (TDM) found in literature [3], a key parameter in the determination of residual stresses. Material constants output from MCQ-Composites formed part of a ABAQUS user subroutine (UMAT), which was used to predict the expected residual stresses in a manufactured AM part by use of the software GENOA.

GENOA uses a three-phase process: (1) a thermal simulation, to establish a (both) time-and-position-dependent temperature field for the AM part, (2) a simulation to predict residual stress, given temperature data in conjunction with a

temperature-dependent coefficient of thermal expansion and TDM, (3) a service loading simulation follows to predict the mechanical response, given both the predicted level of residual stresses, and the anticipated loading conditions.

3 MCQ-CHOPPED

The ultimate tensile strength (UTS) and the ultimate compressive strength (UCS) of PLA were assumed to be 60 MPa and 110 MPa, respectively [4], [5]. An ultimate shear strength (USS) assumption was based on an empirical estimate relating to tensile strength [6].

Cylindrical voids parallel to the raster orientation were assumed to exist with a 3.5% volume ratio giving rise to directional dependent strengths of 59.8 MPa in the 11-direction, and 52.7 MPa in the 22 and 33-directions. A stepwise algorithm then matched the rate of strength degradation with increasing strain to tensile data. Data was reduced to the minimum necessary number of points without failing to capture the characteristic of the stress-strain response, as the algorithm evaluates the coefficient of correlation at each point set. From the rate of degradation in tension, micromechanics algorithms and homogenization techniques (Mori-Tonaka and Eshelby failure theories [7]) predict the rate of degradation in the other loading modes (compression, shear, varieties of combined loading), allowing construction of an efficient model for predicting the stress-strain response for an arbitrary load case.

4 MCQ-COMPOSITES

MCQ-composites estimated the TDM via a cure kinetics algorithm which calculated TDM given pre-exponential factors and activation energies [8]. Figure 3 shows the comparison of predicted and empirically measured TDM [3]:

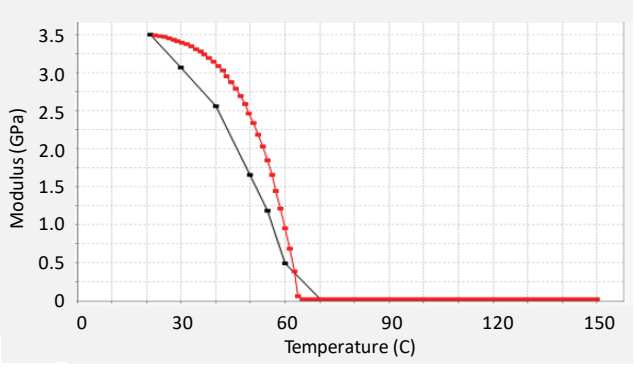

Figure 3: Modulus versus temperature for PLA, (Black squares: empirical data, red squares: predicted)

As the above noted approach is computationally intensive, a multifactor approach was favored, where, at each temperature, applicable mechanical properties were degraded according to the following relationship [1]:

$$\sigma = \sigma_0 \cdot \left(\frac{T_g - T}{T_g - T_0} \right)^{\alpha} \qquad (1)$$

In Equation (1), σ is the degraded property, σ_0 is the property at ambient temperature, T_0 is the ambient temperature, T_g is the glass transition (60°C), and T is the temperature of interest. The multifactors, α, are determined to match the TDM given by cure kinetics. The multifactor approach only holds valid: a.) below the glass transition temperature, and b.) when all three direction-dependent moduli match the corresponding moduli by cure kinetics. The predicted properties and stress-strain responses at each temperature interval populated a ply definition, and were exported to a UMAT card, which was appended using a text editor. Conductivity entries were given by reading temperature-dependent conductivity into MCQ-Chopped [9], producing a temperature-and-direction-dependent matrix of values. The temperature dependence of density [10], specific heat [10], and coefficient of linear thermal expansion [11] entries are all captured from literature. The base plate was defined using a section of a UMAT card for another material (ABS-CF13) as a template, replacing the definitions of the steel base plate used in the tutorial with one of borosilicate glass [12].

5 GENOA

The UMAT card was one of two file-based inputs to the graphic user interface (GUI) in GENOA. The second being the g-code for the AM part. Several input parameters were given by geometry (following the right-hand coordinate system common to all AM printers): the mesh divisions in x were taken to capture one full raster width, and the divisions in y were taken to define a uniform mesh. The number of elements in the layer with the largest footprint defined the lumped elements, and the heating step ratio was taken as the ratio of element print time over layer print time. The ambient and transmission coefficients required initial estimates and a calibration process to match the gradient given by a thermal imaging camera (Shown in Figure 4).

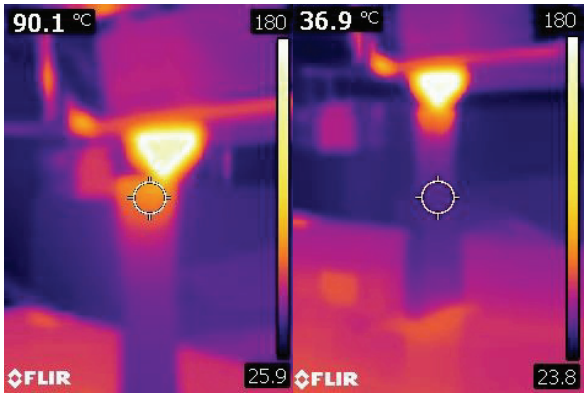

Figure 4: Temperature in an AM process at (left) 2.5 mm from the current layer, and at (right) the steady state layers

The GUI derived a mesh for the part, and generated input files for a thermal simulation, and a residual stress simulation. The gradient shown in Figure 4 was matched by adjustment of the initial estimates of the ambient temperature and the transmission coefficients, followed by sucessive simulations of the 1:1 geometry observed in Figure 4, giving rise to the gradient and input parameters shown in Figure 5.

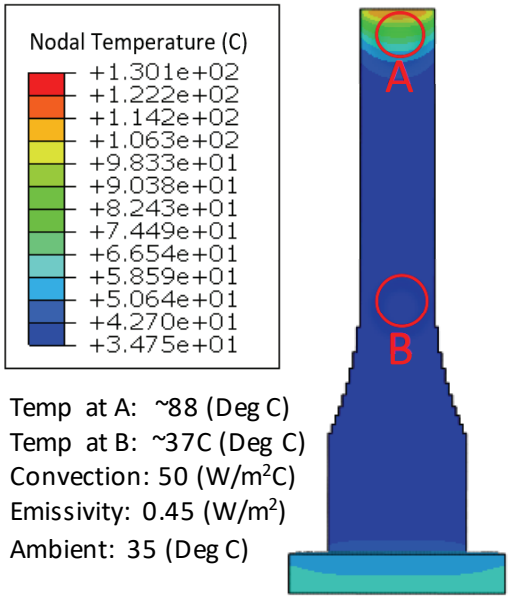

Figure 5: Predicted Thermal Field in a ½-scale ASTM D638 Type IV Tensile Specimen [13] During Printing

The thermal field and residual stresses for three 1/8-scale specimen were then simulated, predicting stress for specimen with loading a.) along raster direction, b.) loading transverse to raster direction (both shown in Figure 6), and c.) loading out-of-plane with respect to raster direction. (cf. Figure 7)

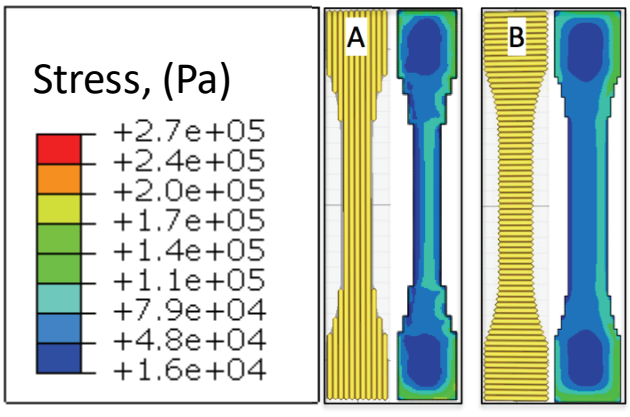

Figure 6: Predicted residual stress shown adjacent to corresponding raster orientation in a tensile specimen for layers with A.) longitudinal rasters, and B.) transverse rasters

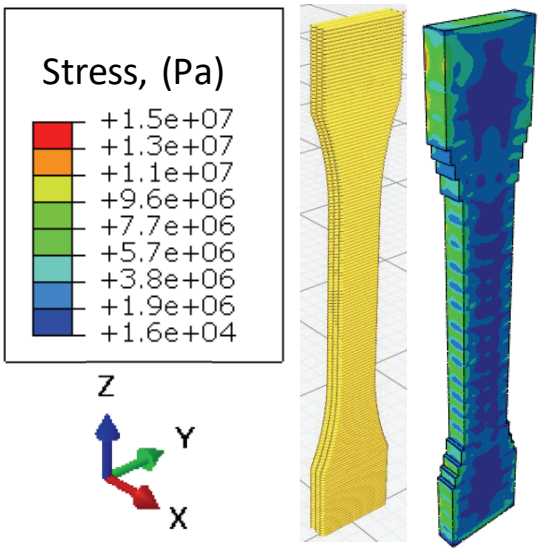

Figure 7: Predicted residual stress shown adjacent to corresponding raster orientation in a vertical tensile specimen

The stress state in Figure 7 is fed forward to a service loading simulation as an initial condition, and is strained to fracture. The service loading simulation is a geometric duplicate of the mesh used for the residual stress simulation (absent the element definitions for the base plate). The service loading simulation is given a simplified material definition, as a temperature dependent definition is no longer needed, and is executed as a mass-scaled, dynamic, explicit simulation. Fracture is seen to occur at 49.4 MPa in the case of specimen with longitudinally oriented rasters (shown in Figure 6, A), 41.1 MPa in the case of specimen with transverse rasters (shown in Figure 6, B), and 42.9 MPa for specimen loaded along layer boundaries (shown in Figure 7).

Characteristically, all orientations simulated seemed to exhibit the same fracture pattern, breaking at the end of the gauge length. A vertically oriented specimen, loaded along layer boundaries is shown below, in Figure 8:

Figure 8: Fracture of a section along the gauge length of a vertically oriented tensile specimen

6 RESULTS AND DISCUSSION

A comparison of the results from simulated tensile fracture to the analytically predicted response given by MCQ is shown below, in Figure 9:

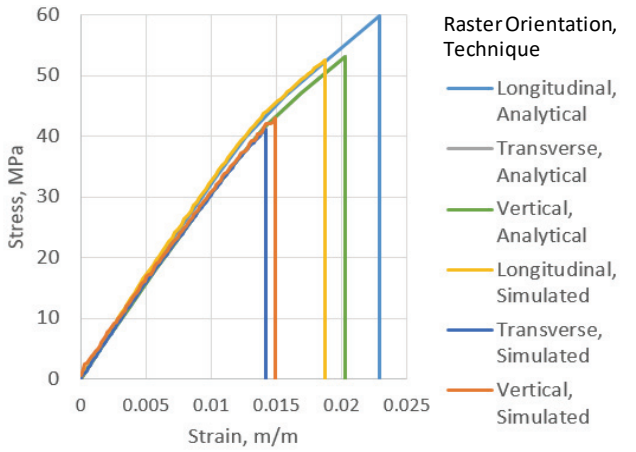

Figure 9: A comparison of analytically predicted stress-strain response (given by MCQ-Chopped) to simulated tensile fracture (given by GENOA in conjunction with ABAQUS)

These results are highly preliminary, and, as with all FEA-based predictions, need to be evaluated for solution convergence with mesh refinement. Additionally, as the fundamental basis for stress derivation sources from thermal expansion, a degree of length dependency is expected, so consistently sized specimen must be compared to expect a comparable result. Before the result from thermal imaging camera may be deemed reliable, the emissivity settings need calibration, and the degreee of error from the parallax effect must either be established, or eliminated by seeking a more favorable camera angle. Despite all these caveats, the tensile response is seen to match quite well, the only disagreement is seen at UTS. The simulation under-predicts the analytically predicted fracture strength by 15-20%.

Additionally, all simulated fractures appear to under-predict independently collected experimental data, as longitudinally evaluated specimen were seen to fail between 55-60 MPa, transverse specimen were seen to fail at 53-59 MPa, and vertical specimen were seen to fail at 43-48 MPa.

The stress pattern given by the residual stress analysis seems to indicate a higher stress pattern when building taller objects with numerous layers, but despite feeding the residual stresses forward to the service loading simulation, the response to transverse raster loading (Figure 6, b) seems to under-perform the response in out of plane loading (Figure 7).

7 CONCLUDING REMARKS

Though stress-strain response of an AM part is generally a fairly simplistic goal to achieve experimentally, numeric simulation of an AM process is much more involved. However, absent a complete definition (including strain-rate dependency), the need for the inclusion of a further necessary mechanism is not yet known.

8 ACKNOWLEDGEMENTS

We would like to thank Dr. Keith Berube for all aspects of aid with experimental verification and validation. We would also like to thank Arshi Sagati, Dr. Harsh Baid, Dr. Frank Abdi, and all the other supporting Alphastar staff.

9 REFERENCES

[1] N. Moazami, H. Baid, S. Dormohammadi, C. Godines, F. Abdi, and G. P. Tandon, “Prediction and Validation of Thermal Mechanical Properties of 3D Printed Ultem 1010,” 2018.

[2] M. R. Talagani, S. Dormohammadi, R. Dutton, C. Godines, H. Baid, and F. Abdi, “Numerical Simulation of Big Area Additive Manufacturing (3D Printing) of a Full Size Car,” 2015, pp. 27–36.

[3] C. Zhou *et al*., “Temperature dependence of poly(lactic acid) mechanical properties,” *RSC Adv*., vol. 6, no. 114, pp. 113762–113772, 2016.

[4] N. LLC, “Ingeo ™ Biopolymer 2003D.” pp. 1–3.

[5] T. Yamamura, M. Omiya, T. Sakai, and P. Viot, “Evaluation of Compressive Properties of PLA / Pbat Polymer Blends,” *Asian Pacific Conf. Mater. Mech*., pp. 3–6, 2009.

[6] J. Torres, J. Cotelo, J. Karl, and A. P. Gordon, “Mechanical property optimization of FDM PLA in shear with multiple objectives,” *Jom*, vol. 67, no. 5, pp. 1183–1193, 2015.

[7] H. K. Baid, F. Abdi, M. C. Lee, and U. Vaidya, “SAMPE 2015 , Baltimore MD Chopped Fiber Composite Progressive Failure Model under Service Loading,” pp. 1–17, 2015.

[8] J. Vogel, “Activation Energy for Diffusion and Welding of PLA films,” *Polym. Eng. Sci*., 2012.

[9] S. Farah, D. G. Anderson, and R. Langer, “Physical and mechanical properties of PLA , and their functions in widespread applications — A comprehensive review,” *Advanced Drug Delivery Reviews*. Elsevier B.V., 2019.

[10] Moldflow Plastics Labs, “Moldflow Material Testing Report MAT2238 NatureWorks PLA,” 2007.

[11] E. José, P. Júnior, R. D. P. Soares, N. Sérgio, and M. Cardozo, “Analysis of equations of state for polymers,” *Sci. Tech*., vol. 25, no. 3, pp. 277–288, 2015.

[12] DURAN inc, “Properties of Borosilicate Glass.” pp. 16–17.

[13] ASTM D 638 -02a, “Standard test method for tensile properties of plastics,” *ASTM D 638 -02a*, vol. 08, pp. 46–58, 2003.